

Natural Radioactivity and Radioelement Potentially of Mylonite Rocks in Nugrus Area, Southeastern Desert, Egypt

A. H. Oraby^a, G. M. Saleh^b, E. M. Hassan^a, S. E. Eldabour^b,
A. M. El Tohamy^b, M. S. Kamar^b,
M. G. El Feky^b, and A. El Taher ^{c,d,*}

^a Department of Physics, Faculty of Science, Aswan University, Aswan, Egypt

^b Nuclear Materials Authority, El Maadi, Cairo, Egypt

^c Physics Department, Faculty of Science, Al-Azhar University, Assuit, Egypt

^d Department of General Educational Development, Faculty of Science and Information Technology,
Daffodil International University, Ashulia, Dhaka-1341, Bangladesh

*e-mail: atef.eltaher@gmail.com

Received August 24, 2022; revised October 20, 2022; accepted October 27, 2022

Abstract—The present study focuses on the distribution of natural radionuclides and the determination of radioelement favorability in the Nugrus mylonite rock. The radionuclide contents were measured with a NaI(Tl) detector. The concentrations of U, Th, Ra (in terms of eU), and K in the mylonite studied range from 27 to 247 ppm, from 96 to 377 ppm, from 11 to 166 ppm, and from 1.14 to 3.12%, with the averages of 100 ppm, 201 ppm, 55 ppm, and 2.1%, respectively. The interelement relationships indicate that the radioelement distribution is not only magmatic but also hydrothermal. Variations of migration parameters for uranium indicate fluctuations in physicochemical conditions that lead to U accumulation and leaching processes, which are confirmed by increments and decrements in uranium concentrations. The examined samples demonstrate disequilibrium, with eU/Ra (eU) ranging from 1.32 to 3.26, with an average of 1.95, which suggests uranium addition. Uranium, thorium, and potassium favorability indices of the investigated mylonite rocks indicate moderate favorability of these rocks for uranium and thorium and high favorability for potassium. The *F*-parameter illustrates the presence of different stages of alterations. Mineralogical investigation indicates the presence of such radioactive minerals as thorite and Uranothorite, of Nb-Ta minerals (columbite and ishikawite), and of zircon and xenotime.

Keywords: Wadi Nugrus, radioelements, equilibrium, mylonite, radioactive minerals, uranium favorability

DOI: 10.1134/S1066362222050095

INTRODUCTION

There are three types of radiation in nature: ionizing radiation, non-ionizing radiation, and external radiation. Exposure of a person to ionizing radiation is considered as a scientific subject that attracts public attention, because natural-source radiation accounts for the majority of the overall radiation exposure of the human population [1]. The Earth's environment has widespread natural radiation, which is found in air, water, soil, and plants. The existence of natural radionuclides, such as ^{238}U , ^{232}Th , and ^{40}K , in diverse geological formations causes natural radioactivity in the environment [2]. Gamma rays are released

at high levels from geological formations such as granite, whereas low levels are provided by sedimentary rocks [3–6].

Tawfic et al. [7] studied the concentration of radioactive elements in the north W. Baroud area using a NaI(Tl) detector. They found that the average activity concentrations of ^{232}Th , ^{226}Ra , and ^{40}K were 131 ± 90 , 215 ± 118 , and $822 \pm 125 \text{ Bq kg}^{-1}$, respectively [7]. In the Abu Rusheid area, the average activity concentrations of ^{238}U , ^{226}Ra , ^{232}Th , and ^{40}K were 501.8, 577.8, 692, and 352.6 Bq kg^{-1} , respectively, being higher than the global value [8]. A case study of Wadi Rod Elsayalla has shown that the mean activity concentrations of ^{238}U , ^{232}Th , and ^{40}K are 62.2 ± 20.8 , 84.2 ± 23.3 , and

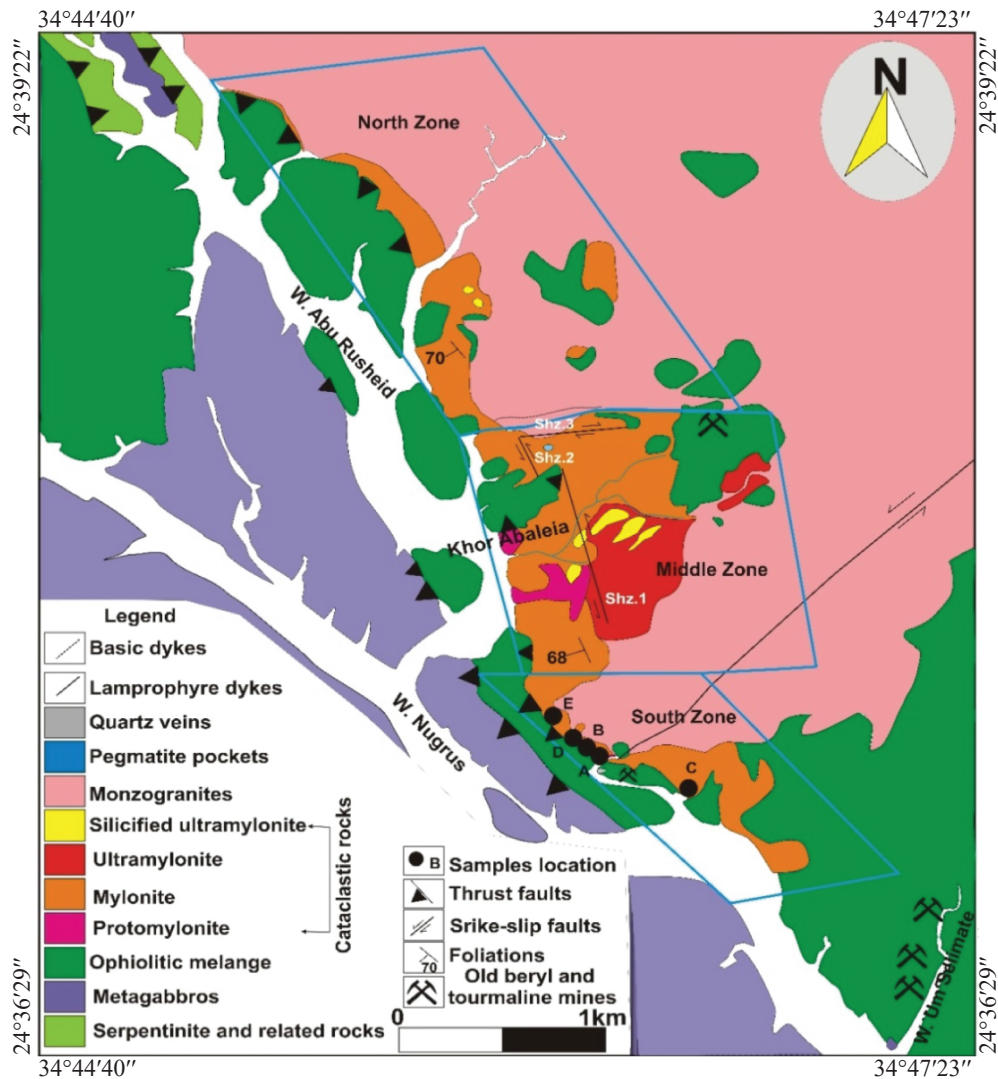


Fig. 1. Geological map of W. Nugrus area, SED, Egypt [11].

949.4 ± 172.5 Bq kg $^{-1}$, being higher than the world average values [9].

This study aims at determining the distribution of natural radionuclides and their potentiality in the Nugrus region, Southeastern Desert, Egypt.

GEOLOGIC SETTING OF NUGRUS AREA

The research region lies in the Southeastern Desert (SED) of Egypt, southwest of Marsa Alam City, between longitudes 34°44'40" E and 34°47'23" E and latitudes 24°36'29" N and 24°39'22" N (about 45 km SW Marsa Alam). It is accessible by the Sheikh Salem–Sheikh El-Shazly highway asphaltic road or the Wadi (W.) El Gemal entry along the Red Sea shore. The 35-kilometer-long NW-trending W. Nugrus shear zone, which is one

of the major shear zones in the Najd Fault Corridor, is included in the study area (NFC) [10].

The tectonostratigraphic sequence of the Precambrian rocks of W. Nugrus area (Fig. 1) is arranged from base to top as follows: (i) ophiolitic mélange consisting of ultramafic rocks and layered metagabbros set in the metasediment matrix; (ii) cataclastic group consisting of protomylonites, mylonites, ultramylonites, and silicified ultramylonites; (iii) granitic rocks; and (iv) post-granite dykes and veins [11].

The cataclastic rocks covering an area of about 2 km 2 are represented by protomylonite, mylonite, ultramylonite, and silicified ultramylonites with gradational contacts, highly sheared, banded (N–S), and cut by two shear zones (NNW–SSE and E–W trends). The shear zones range from 2 to 10 m in width and

from 400 to 1500 m in length with vertical dip and are extruded by lamprophyre dykes. The dykes are a good physical and chemical trap for U, REEs, Cu, Zn, Ag, Pb, and Y. The mineralized cataclastic rocks can be divided into three zones: the north, middle, and south zones. The present study focuses on the south zone of the mineralized cataclastic rocks, which is represented by mylonite rock. The mylonite covers a large area representing 65.0 vol % of the cataclastic rocks with low to medium relief [11]. They are fine to medium-grained and well banded (NNW–SSE and dips 10°/WSW). These rocks are intercalated with protomylonite and affected by weathering in variable degrees producing red to yellow colors due to the alteration of sulfides producing iron oxides (hematite-limonite).

MATERIALS AND METHODS

Fifty samples from the mylonite rocks of W. Nugrus were collected from different locations and then crushed and ground into powder. After that, they were packaged in a plastic container and closed tightly to prevent the leakage of radon and then stored for 4 weeks to reach secular equilibrium, in which the decay rates of the daughter nuclides and their respective parents become the same.

The γ -ray spectrometry system consists of a Bicron scintillation detector, NaI(Tl) crystal, 76 × 76 mm, hermetically sealed with a photomultiplier tube in aluminum housing. The detector is masked with its amplifier in a copper shield (0.6 cm thick) against induced X-rays and a cylindrical lead chamber against the environmental radiations and is connected to the Accuspec card. The Accuspec NaI plus 2k on board ADC, Amp, and HVPS with 2k channel memory is attached to the PC board.

The measurement of the radionuclides is based on choosing four energy regions of interest (ROIs) representing ^{234}Th , ^{212}Pb , ^{214}Pb , and ^{40}K for U, Th, Ra, and K, respectively (Table 1). Uranium is estimated both as eU and Ra (eU) and thorium, as eTh. The values of eU represent the concentration of U evaluated using the ^{234}Th energy peak (93 keV); ^{234}Th is the first daughter isotope in the ^{238}U decay series with very low possible loss. Radium is measured by the ^{214}Pb energy peak (352 keV), which is considered as a measure of the U concentration only in the case of the secular equilibrium

Table 1. Energy regions of interest (ROIS) for U, Th, Ra, and K analysis of rock samples [12]

ROI	Element	Determined by daughter nuclide	Peak energy, keV	Channels
1	U	^{234}Th	92.60	77–103
2	Th	^{212}Pb	238.6	218–270
3	Ra	^{214}Pb	352.0	329–389
4	K	^{40}K	1460.0	1290–1422

between ^{238}U and all its daughter isotopes. Thorium is measured by the ^{212}Pb energy peak (238 keV).

The quality of the results obtained depends on many factors, namely: (i) size and energy resolution of the scintillation detector, (ii) sample mass and geometry, (iii) detector shielding, (iv) performance and operation stability of the multichannel analyzer, (v) selection of specific detected γ -ray energies, (vi) measurement time, (vii) quality and reliability of the standards used, and (viii) data processing method.

The radionuclide measurement includes three main steps: energy calibration, sensitivity calibration, and γ -ray assaying.

Energy Calibration

The energy stability of the spectrometer channels varies with changes in the power supply, voltage, and amplification characteristics of the photomultiplier tube. Both power supply and photomultiplier characteristics are dependent upon temperature. To ensure that the instrument accurately records the γ -radiation energy of the radioactive elements, permanent calibration was carried out by using radioactive calibration sources, ^{137}Cs (661.6 keV, set up in channel 662) and ^{57}Co (122.1 keV, set up in the channel 122), as follows: Calibration is started with the ^{137}Cs source (gain adjustment) and then with ^{57}Co source (zero adjustments). Then, the ^{137}Cs source is repeatedly used as a minimum procedure.

Sensitivity Calibration

Since the γ -ray spectrometer is used in geochemical prospecting, it should be calibrated in terms of the isotopic sensitivity (i.e., conversion from counts per unit

Table 2. Effective concentrations (per unit mass) of radioelements in the standards of U, Th, Ra, and K [12]

Standard	U, ppm	Th, ppm	Ra, ppm	K, %	Mass, g
NMA-U	1023.0	1.60	4.18	0.20	369.1
IAEA-Ra	400.0	0.62	392.00	0.00	330.7
IAEA-Th	6.3	800.00	6.30	0.02	314.2
IAEA-K	0.00	0.00	0.00	44.80	335.8

of time into isotopic concentration in parts per million or percents). The calibration was carried out using four artificial standard sources (geological reference materials). These standards were prepared from a series of certified reference samples with certain U, Th, and K concentrations, obtained from IAEA [12]. The effective concentrations of radioelements in these standards and the masses of the standards are given in Table 2.

The sensitivity of the equipment used was determined by measuring four standards two times, 1000 s for each, and then taking the averages of the gross counts recorded in the selected ROIs. Enumeration of count rates was corrected for background count rates in the ROIs and normalized per unit mass. The corrected values were input into the Analysis computer program that was developed for laboratory γ -ray spectrometry of geological materials [12].

The result is a matrix of sensitivity values of the equipment; each of them is expressed by the count rate per unit radioelement. These sensitivity values of the equipment are used as a reference in the analysis of unknown rock samples.

γ -Ray Assaying

After preparing the samples, they were subjected to γ -ray assaying. It included the following steps:

(1) equipment setup using reference γ -emitting sources (^{137}Cs and ^{57}Co) for energy calibration;

(2) assaying of the samples by 1000-s counting in the shielded environment and determination of the gross counts for U, Th, eU (Ra), and K at their selected energy regions;

(3) determination of the background count rates in the selected energy regions (ROIs) for the laboratory with the detector;

(4) processing of the registered spectrometric data (gross counts for eU, eTh, Ra, and K) for each sample with the Analysis computer program using the background count rates, sample weight, measurement time, and the preliminary sensitivity constants to determine the U, Th, and Ra concentrations in parts per million (ppm) and the K concentration in percents (%).

The crushed samples were ground, quartered, and sieved; the 0.125–0.250 mm size fraction was washed and separated using bromoform, and its heavy fraction was subjected to the magnetic fractionation using a Frantz Isodynamic magnetic separator (model LB 1).

Binocular microscopes were used to identify minerals, which were then identified using an environmental scanning electron microscope (ESEM, model Philips XL 30) with an energy-dispersive spectrometer (EDX) unit at an accelerating voltage of 25–30 kV, a beam diameter of 1–2 mm, and a counting time of 60–120 s.

RESULTS AND DISCUSSION

Mineralogical Investigation

The binocular microscopic and ESEM investigation showed that Nugrus rocks were made up of the following major mineral assemblages.

Thorium minerals. *Thorite* [ThSiO_4] occurs as anhedral fine to very fine blackish opaque crystals. Thorite grains were confirmed by ESEM, and the analysis data show that the mineral is composed mainly of Th (77.8 wt %), U (10.28 wt %), and Si (8.17 wt %), Fig. 2a.

Uranotherorite [$(\text{Th}, \text{U})\text{SiO}_4$]. According to [12], uranium is usually present in amounts of up to ~10% in this mineral. This is confirmed by ESEM. Analysis results show that the mineral contains Th (70–64.3 wt %), U (11–16.6 wt %), and small amounts of Y, Figs. 2b and 2c. Also, it was found as a solid solution associated with zircon, Fig. 2d.

Nb-Ta minerals. *Columbite mineral* [(Fe,Mn,Mg)(Nb,Ta) $_2$ O $_6$] is the most widespread niobium mineral. This is an important ore of the industrially useful metal. Columbite, also called niobite, consists of black to dark brown tabular or prismatic crystals; it crystallizes in the orthorhombic system. Columbite was confirmed by the ESEM technique. It contains Nb (68–57.6 wt %), Ta (7.4–9.3 wt %), Fe (13.3–12.75 wt %), and Σ HREEs (0.76–3 wt %). The Nb/Ta ratio equal to 9–6.2 shows enrichment in Ta, Figs. 3a and 3b. Also, columbite was associated with uranotherorite on the quartz surface, Fig. 3c.

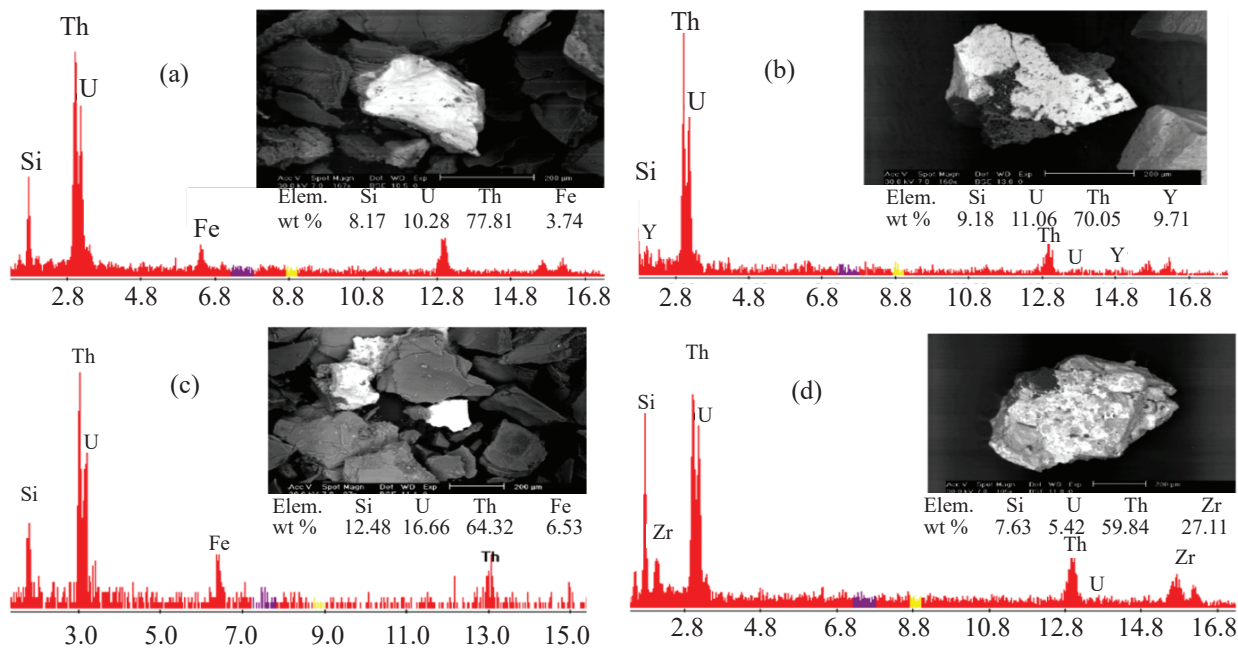


Fig. 2. BSE images and EDX patterns of (a) thorite and (b-d) uranothorite minerals, W. Nugrus, SED, Egypt.

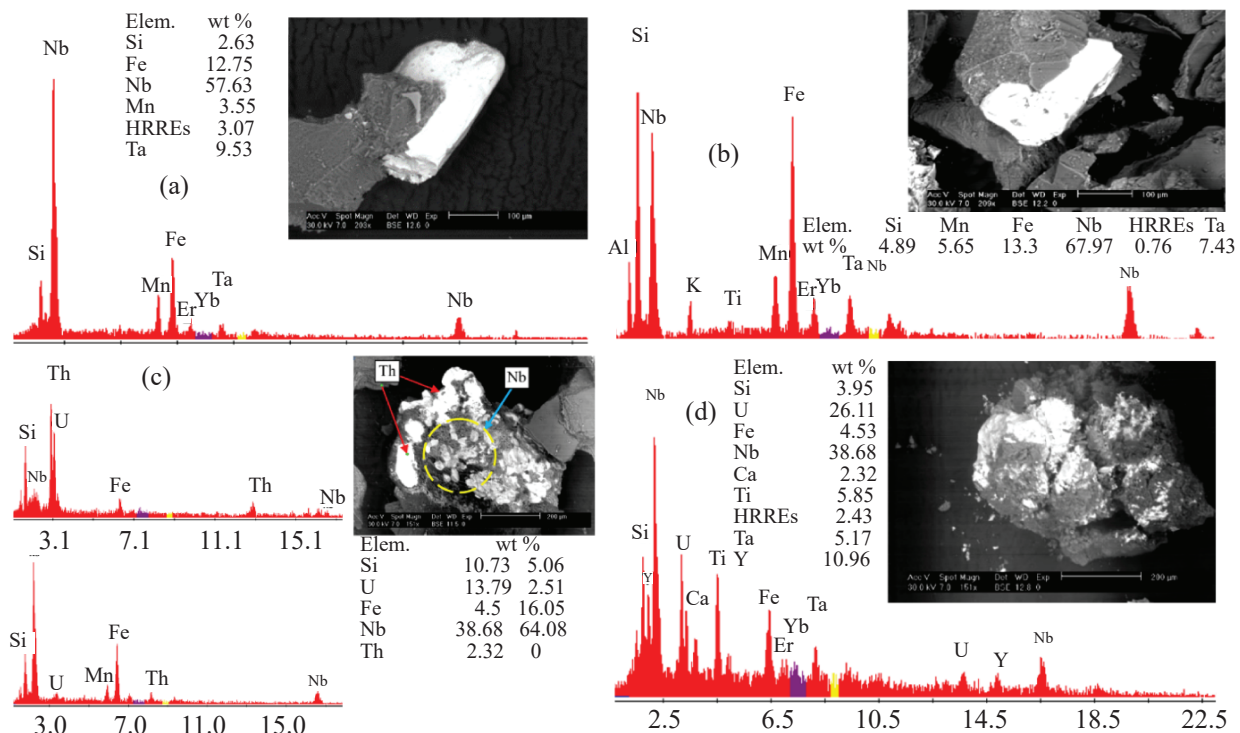


Fig. 3. BSE images and EDX patterns of (a-c) columbite and (d) ishikawaite minerals, W. Nugrus, SED, Egypt.

Ishikawaite $[(\text{U}, \text{Fe}, \text{Y}, \text{Ca})(\text{Nb}, \text{Ta})\text{O}_4]$. Černý and Ercit [13] describe ishikawaite as a probable uranium-rich variety of samarskite. It exists in the form of angular to subangular grains and consists of Nb

(38.6 wt %), U (26 wt %), Y (11 wt %), and HREEs (2.4 wt %), Fig. 3d.

Accessory minerals. Zircon (ZrSiO_4) is a common accessory mineral in nature. Zirconium finds diverse

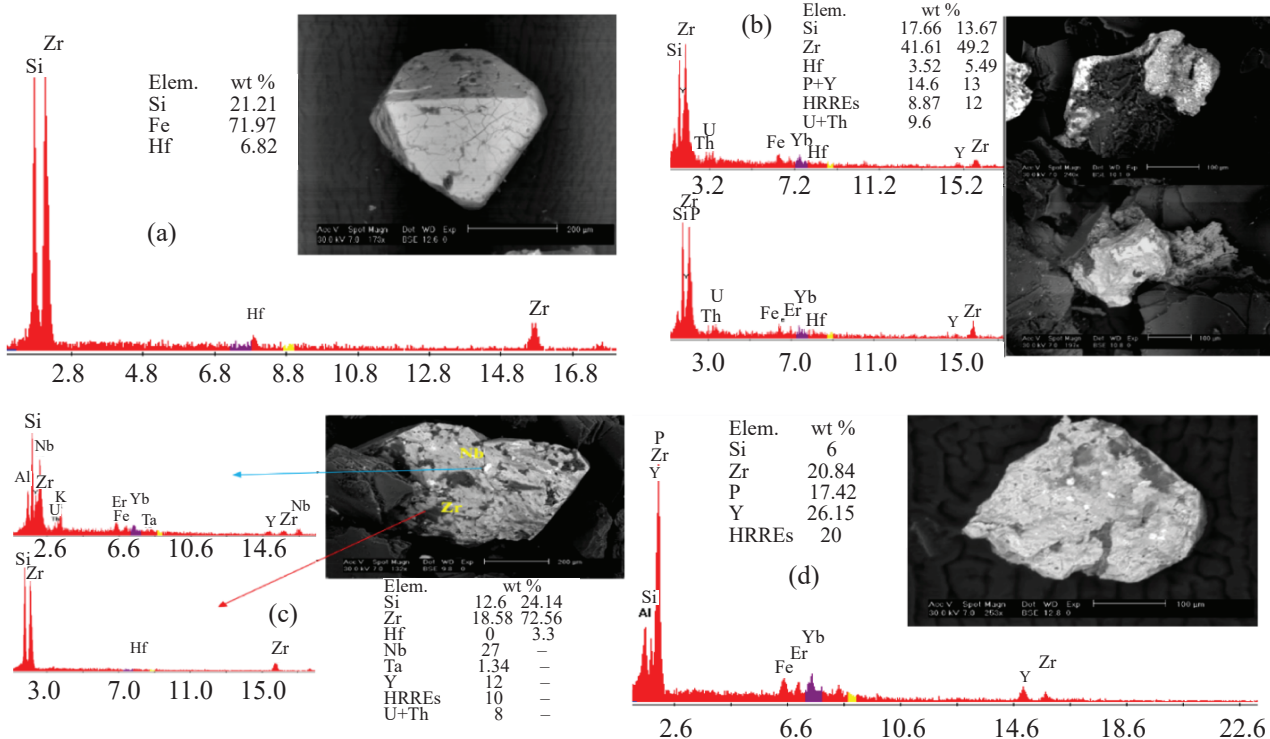


Fig. 4. BSE images and EDX patterns of (a–c) zircon and (d) xenotime minerals, W. Nugrus, SED, Egypt.

industrial applications because it is highly resistant to corrosion. In particular, it is used in nuclear reactor pumps, valves, and cores. Metamictization of natural zircon is generated by the radioactive decay of trace quantities of U and Th substituting for Zr, which causes accumulated radiation damage to the crystal structure. The damage is thought to be caused by recoil nuclei generated by α -decay [14]. Metamictization involves considerable changes in physical parameters, such as density, refractive index, and birefringence [15]. The EDX analyses of zircon give a Zr/Hf ratio of 10.5, Fig. 4a. Zircon is also found as a solid solution with other minerals such as xenotime and columbite, Figs. 4b, 4c.

Xenotime (YPO_4) crystals are similar to zircon and can easily be confused. They have duller luster. Often uranium or other rare elements such as erbium, thorium, ytterbium, zirconium, and the not-so-rare calcium are found as traces in xenotime, replacing yttrium. The EDX analyses demonstrate the presence of Y (26 wt %), P (17.4 wt %), and HREEs (20.8 wt %), Fig. 4d.

Radioelement Distribution

The radioelement concentrations in the mylonite studied are as follows: U from 27 to 247 ppm, Th from

96 to 377 ppm, Ra (eU) from 11 to 166 ppm, and K from 1.14 to 3.12%, with the averages of 100, 201, 55 ppm, and 2.07%, respectively (Table 2). These rocks are considered uraniferous, as they have more than twice the Clark value (4 ppm) according to [16–18]. The high radioactivity is due to the presence of thorite and uranothorite minerals.

The eTh/eU ratios in igneous rocks are (3–4) : 1 according to [9, 19]. The eTh/eU ratio is crucial for U exploration by determining U-rich locations, and it is based mostly on the content of U. Low ratios (<3.5) in granites suggest U enrichment (addition of U) [20], whereas high ratios (>3.5) suggest uranium leaching-out [21]. In the mylonite studied, the eTh/eU ratio varies from 1 to 4.11 with 2.22 as an average (Table 1). This average is lower than the natural ratio in granitic rocks (3.5), which can be attributed to the U fertility in these rocks.

Geochemistry of Radioelements

The correlation between Th, U, and their ratios may be associated with the physicochemical conditions in the period when these elements were mobilized [22, 23]. The eTh–eU cross plot demonstrates moderate correlation (0.55), suggesting that magmatic processes play a significant role in the radioelement distribution in

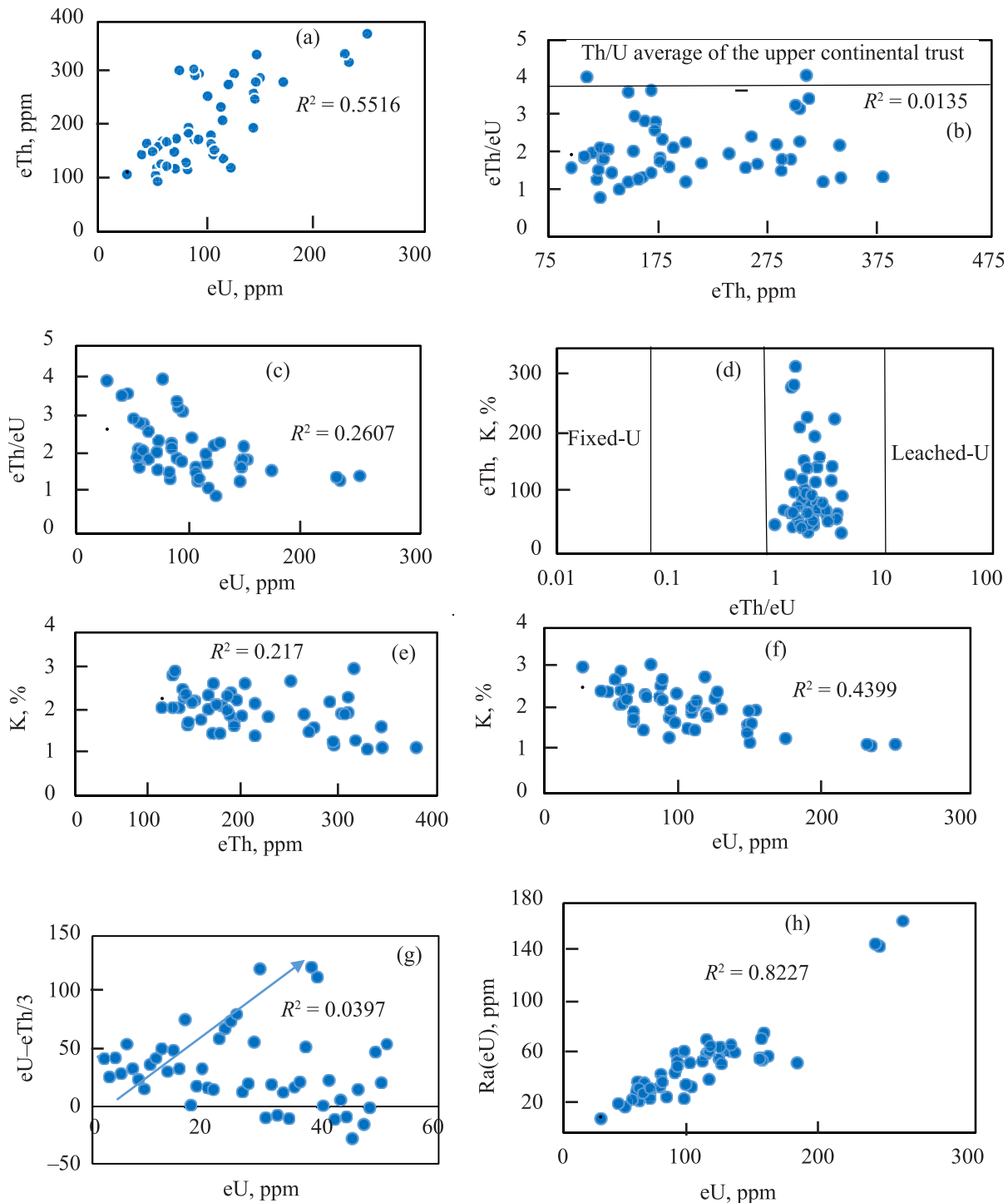


Fig. 5. (a) eU-eTh, (b) eTh-eTh/eU, (c) eU-eTh/eU, (d) eTh/eU-eTh/K, (e) eTh-K, (f) eU-K, (g) eU-(eU - eTh/3) and (h) eU-Ra(eU) correlations for the mineralized mylonite rock studied, W. Nugrus, SED, Egypt.

the rock studied, Fig. 5a. As seen from Fig. 5b, most of the samples lie below the line represented the Th/U average of continental crust, confirming uranium enrichment in these rocks. On the other hand, the relationships of

eTh and eU with the eTh/eU ratio are ill-defined and weakly negative, respectively, which indicates that late hydrothermal processes also control the distribution of the radioelements, Figs. 5b and 5c.

Table 3. Radionuclide concentrations and ratios in the samples^a

Sample code	eU, ppm	eTh, ppm	Ra(eU), ppm	K, %	eTh/eU	eU/eTh	eU/Ra(eU)	eTh/K	eU – eTh/3
S1-1	82	119	62	2.6	1.45	0.69	1.32	45.77	42.33
S1-2	120	281	64	2.3	2.34	0.43	1.88	122.17	26.33
S1-3	114	213	67	1.94	1.87	0.53	1.7	109.79	43.00
S1-4	88	176	64	1.83	2	0.5	1.38	96.17	29.33
S1-5	143	264	59	1.66	1.85	0.54	2.42	159.04	55.00
S1-6	113	238	58	2.81	2.11	0.47	1.95	84.7	33.67
S1-7	125	302	63	2.04	2.42	0.41	1.98	148.04	24.33
S1-8	54	115	40	2.15	2.13	0.47	1.35	53.49	15.67
S1-9	81	132	47	2.33	1.63	0.61	1.72	56.65	37.00
S1-10	104	184	62	1.96	1.77	0.56	1.68	93.88	42.67
S1-11	149	294	60	2.01	1.97	0.51	2.48	146.27	51.00
S1-12	71	120	46	2.39	1.69	0.59	1.54	50.21	31.00
S1-13	145	286	57	1.23	1.97	0.51	2.54	232.52	49.67
S1-14	146	338	78	1.69	2.32	0.43	1.87	200	33.33
S1-15	143	199	58	1.47	1.39	0.72	2.47	135.37	76.67
S1-16	59	172	39	2.52	2.92	0.34	1.51	68.25	1.67
S1-17	54	108	33	2.96	2	0.5	1.64	36.49	18.00
S1-18	92	176	55	1.71	1.91	0.52	1.67	102.92	33.33
S1-19	83	199	56	2.26	2.4	0.42	1.48	88.05	16.67
S1-20	101	258	56	1.57	2.55	0.39	1.8	164.33	15.00
S1-21	144	253	74	1.99	1.76	0.57	1.95	127.14	59.67
S1-22	115	139	54	1.86	1.21	0.83	2.13	74.73	68.67
S1-23	170	285	55	1.32	1.68	0.6	3.09	215.91	75.00
S1-24	122	122	69	2.45	1	1	1.77	49.8	81.33
S1-25	54	122	35	2.49	2.26	0.44	1.54	49	13.33
S1-26	83	188	52	2.75	2.27	0.44	1.6	68.36	20.33
S1-27	106	147	64	2.12	1.39	0.72	1.66	69.34	57.00
S1-28	247	377	166	1.18	1.53	0.65	1.49	319.49	121.33
S2-1	27	110	11	3.05	4.07	0.25	2.45	36.07	-9.67
S2-2	70	152	36	1.53	2.17	0.46	1.94	99.35	19.33
S2-3	93	302	36	2.41	3.25	0.31	2.58	125.31	-7.67
S2-4	72	178	40	2.34	2.47	0.4	1.8	76.07	12.67
S2-5	89	298	38	2	3.35	0.3	2.34	149	-10.33
S2-6	53	108	32	2.15	2.04	0.49	1.66	50.23	17.00
S2-7	63	124	30	1.73	1.97	0.51	2.1	71.68	21.67
S2-8	106	160	42	1.53	1.51	0.66	2.52	104.58	52.67
S2-9	230	323	146	1.14	1.4	0.71	1.58	283.33	122.33
S2-10	227	339	148	1.18	1.49	0.67	1.53	287.29	114.00
S2-11	55	162	25	2.2	2.95	0.34	2.2	73.64	1.00

Table 3. (Contd.)

Sample code	eU, ppm	eTh, ppm	Ra(eU), ppm	K, %	eTh/eU	eU/eTh	eU/Ra(eU)	eTh/K	eU – eTh/3
S2-12	55	96	35	2.16	1.75	0.57	1.57	44.44	23.00
S2-13	45	168	20	2.45	3.73	0.27	2.25	68.57	-11.00
S2-14	63	171	27	1.97	2.71	0.37	2.33	86.8	6.00
S2-15	40	147	23	2.47	3.68	0.27	1.74	59.51	-9.00
S2-16	75	308	28	3.12	4.11	0.24	2.68	98.72	-27.67
S2-17	58	129	31	2.28	2.22	0.45	1.87	56.58	15.00
S2-18	88	310	27	1.35	3.52	0.28	3.26	229.63	-15.33
S2-19	50	153	26	2.75	3.06	0.33	1.92	55.64	-1.00
S2-20	104	168	73	2.09	1.62	0.62	1.42	80.38	48.00
S2-21	63	125	35	1.8	1.98	0.51	1.8	69.44	21.33
S2-22	107	156	68	2.23	1.46	0.68	1.57	69.96	55.00
Minimum	27	96	11	1.14	1	0.24	1.32	36.07	-27.67
Maximum	247	377	166	3.12	4.11	1	3.26	319.49	122.33
Average	100.29	201.29	54.75	2.07	2.22	0.51	1.95	111.53	32.19

^a Detection limits for all radionuclides are $\pm 10\%$.

The plots of K (%) vs. eU and eTh (ppm) show that there is weak and very weak negative correlation, respectively, between the two radioelements and potassium, Figs. 5e, 5f. This fact suggests uranium migration with the alteration of potassium minerals [9, 23, 24]. The eU vs. (eU – eTh)/3 diagram suggests fluctuations in physicochemical conditions that led to U accumulation and leaching processes; they are confirmed by increments and decrements in uranium concentrations, Fig. 5g.

Radioactive Equilibrium

The equilibrium factor (P) is defined as the ratio of radiometrically measured uranium content (eU) to the radium equivalent uranium content (P -factor = eU/Ra(eU)). This parameter can be used to evaluate the radioactive equilibrium in the area under investigation, which was suggested in [26] and applied in [19, 22, 23, 27]. If the P -factor is greater than or less than unity, uranium is added or removed. The addition

and removal of uranium are attributed to particular geological processes, such as alteration, which disrupt the equilibrium state. The examined samples show disequilibrium conditions, with eU/Ra(eU) ranging from 1.32 to 3.26 with an average of 1.95, indicating uranium addition (Table 3, Fig. 5h).

The migration parameter or authigenic U can be computed as $U_{(ppm)} - Th_{(ppm)}/3$. All samples in Nugrus mylonite have positive values of this parameter, suggesting U accumulation in the study area.

Radioelement Favorability

The encouraging environments for U deposits are generally found and recognized depending on geologic, structural, mineralogical, geochemical, and radiometric features [28–30]. The U-rich granites should have high U content (>10 ppm) and a low Th/U ratio (<2); alteration processes play a significant role in U leaching and concentration in structural traps to produce a uranium deposit.

Table 4. U, Th, and K favorability indices and F -parameter of the altered granites studied

Value	eU, ppm	eTh, ppm	K, %	UFI	ThFI	KFI	F -Parameter
Minimum	27	96	1.14	1.60	0.38	974	0.38
Maximum	247	377	3.12	12.81	2.45	78914	2.45
Average	100	201	2.1	4.16	1.03	9739	1.03

In the present study, U, Th, and K favorable rocks are recognized depending chiefly on the radiometric information using the following equations [31].

Uranium favorability index (UFI):

$$UFI = \text{MeTh} \times MK/\text{MeU};$$

Thorium favorability index (ThFI):

$$ThFI = \text{MeU} \times MK/\text{MeTh};$$

Potassium favorability index (KFI):

$$KFI = \text{MeTh} \times \text{MeU}/MK.$$

Uranium favorability. The values of the uranium favorability index can be partitioned into three assemblages of minor ($UFI \leq 3$), medium ($UFI = 3-5$), and major ($UFI > 5$) potentials. In the mylonite studied, the uranium favorability index values range from 1.60 to 12.81 with the average of 4.16, suggesting that the mylonite studied lies in the moderate uranium favorability assemblage (Table 4).

Thorium favorability. The values of the thorium favorability index can be subdivided into three assemblages of minor ($TFI \leq 1$), medium ($TFI = 1-2$), and major ($TFI \geq 2$) potentials. In the mylonite studied, the thorium favorability indices vary between 0.38 and 2.45 with an average of 1.03, which corresponds to moderate thorium favorability rock types (Table 4).

Potassium favorability. The rocks studied are categorized into two assemblages of potassium-favorable areas depending on their deliberate potassium favorability index [31]: medium potential ($KFI = 10-50$) and major potential ($KFI > 50$). For the mylonite studied, the potassium favorability index falls in the range between 974 and 78914 with an average of 9739. These values lie in the major potential potassium favorability assemblage (Table 4).

F-Parameter. The *F*-parameter characterizes the extent of the alteration of diverse rock units that organize conditions of uranium mobilization and, correspondingly, the possibility of uranium enrichment. The value of this parameter is generally 1.2 or 1.3 and can reach up to 5–10 in extraordinary settings [32]. This parameter is extremely important. It depends on two foremost radiometric characteristics of rocks: abundance of U relative to Th/K ratio and abundance of K relative to Th/U ratio [33]:

$$\text{-parameter } \frac{U}{Th/K} \frac{K}{Th/U}.$$

In the mylonite studied, the *F*-parameter ranges from 0.38 to 2.45, indicating that the rocks studied have different degrees of alteration (Table 4, Fig. 5d).

CONCLUSION

The main outcrops in Nugrus area are ultramafic rocks, layered metagabbros set in a metasediment matrix, cataclastic group, consisting of protomylonites, mylonites, ultramyloites, and silicified ultramyloites, granitic rocks, and post-granite dykes and veins. Radiometrically, the mylonite rocks are considered as high uranium and thorium rocks. Geochemically, the distribution of radionuclides is not only magmatic but also hydrothermal. The increments and decrements of uranium with changes in migration parameters suggest vigorous changes in physicochemical conditions during the mobilization and precipitation of radionuclides. The clear positive disequilibrium between ^{238}U and ^{226}Ra demonstrates uranium addition. These rocks can be categorized as the mineralized type for their low Th/U ratio, high uranium and thorium contents, and rare metal mineralization. Moderate uranium and thorium favorability and high potassium favorability confirm the probability of the presence of both uranium and thorium mineralization, whereas the *F*-parameter illustrates the presence of different stages of alterations. Mineralogical investigation reveals the presence of thorite, uranothorite, columbite, ishikawite, zircon, and xenotime minerals.

REFERENCES

1. *Sources and Effects of Ionizing Radiation, vol. I: Sources*, UNSCEAR Report, 2000.
2. Ghoneim, M.M., Abdel Gawad, A.E., Awad, H.A., Zakaly, H.M.H., Mira, H.I., and El-Taher, A., *Int. J. Environ. Anal. Chem.*, 2021. <https://doi.org/10.1080/03067319.2021.1916006>
3. Abdel Gawad, A.E., Ali, M.A., Ghoneim, M.M., and El-Taher, A., *Int. J. Environ. Anal. Chem.*, 2021. <https://doi.org/10.1080/03067319.2021.1891416>
4. Abdel-Rahman, M.A.E., Sabry, M., Khattab, M.R., El-Taher, A., and El-Mongy, S.A., *Z. Anorg. Allg. Chem.*, 2021, vol. 647, no. 4, pp. 210–217.
5. Ghoneim, M.M., Panova, E.G., Abdel Gawad, A.E.,

- Awad, H.A., Zakaly, H.M.H., and El-Taher, A., *Int. J. Environ. Anal. Chem.*, 2021.
<https://doi.org/10.1080/03067319.2021.1873310>
6. Gawad, A.E.A., Ghoneim, M.M., El-Taher, A., and Ramadan, A.A., *Arab. J. Geosci.*, 2021, vol. 14, 1356.
<https://doi.org/10.1007/s12517-021-07801-0>
7. Tawfic, A.F., Zakaly, H.M.H., Awad, H.A., Tantawy, H.R., Abbasi, A., Abed, N.S., and Mostafa, M., *J. Radioanal. Nucl. Chem.*, 2021, vol. 327, no. 2, pp. 643–652.
8. Gaafar, I., Elbarbary, M., Sayyed, M.I., Sulieman, A., Tamam, N., Khandaker, M.U., Bradley, D.A., and Hanfi, M.Y., *Minerals*, 2022, vol. 12, no. 2, p. 120.
9. Awad, H.A.M., Zakaly, H.M.H., Nastavkin, A.V., and El-Taher, A., *Int. J. Environ. Anal. Chem.*, 2020.
<https://doi.org/10.1080/03067319.2020.1830987>
10. Ibrahim, M.E., Saleh, G.M., Mahmoud, F.O., Abu El Hassan, E.A., Ibrahim, I.H., Aly, M.A., Azab, M.S., Rashed, M.A., Khaleal, F.M., and Mohamed, A.M., *Uranium and Associated Rare Metals Potentialities of Abu Rusheid Brecciated Shear Zone, Southeastern Desert, Egypt*, Internal Report, 2004, part II.
11. Hamimi, Z., El-Fakharani, A., Emam, A., Barreiro, J.G., Abdelrahman, E., and Abo-Soliman, M.Y., *Arab. J. Geosci.*, 2018, vol. 11, article 494.
<https://doi.org/10.1007/s12517-018-3837-3>
12. Matolin, M., *Construction and Use of Spectrometric Calibration pads Laboratory γ -Ray Spectrometry*, NMA, Egypt, Report to the Government of the Arab Republic of Egypt, Project EGY/4/030-03, IAEA, 1991.
13. Černý, P. and Ercit, T.S., *Mineralogy of Niobium and Tantalum: Crystal Chemical Relationships, Paragenetic Aspects and Their Economic Implications, Lanthanides, Tantalum and Niobium*, Berlin: Springer, 1989.
14. Headley, T.J., Ewing, R.C., and Haaker, R.F., *TEM Study of the Metamict State*, Albuquerque, NM (USA): Sandia National Labs., New Mexico Univ., 1982.
15. Holland, H.D. and Gottfried, D., *Acta Crystallogr.*, 1955, vol. 8, no. 6, pp. 291–300.
16. Assaf, H.S., Mahdy, M.A., and El Afandy, A.H. in *3rd Conf. on Geochemistry*, Alexandria Univ., Egypt, 1997, pp. 409–420.
17. Raslan, M.F. and El-Feky, M.G., *Chin. J. Geoch.*, 2012, vol. 31, no. 1, pp. 30–40.
18. El Afandy H., El-Feky, M.G., Taha, S.H., El Minyawi, S.M., Sallam, H.A., Ebyan, O.A., Yousef, E.S., and Hanfi, M.Y., *Minerals*, 2022, vol. 12, article 294.
19. El Feky, M.G., El Mowafy, A.A., and Abdel, A.W., *Chin. J. Geochem.*, 2011, vol. 30, no. 2, pp. 175–186.
20. Salaheldin, G., Tolba, A., Kamel, M., and El-Taher, A., *J. Radioanal. Nucl. Chem.*, 2020, vol. 325, no. 2, pp. 397–408.
21. El-Afandy, A., Mohamed, G.E.-F., Samia, T., El Minyawi, S.M., and Sallam, H.A., *Greener J. Geol. Earth Sci.*, 2016, vol. 4, no. 3, pp. 56–69.
22. El Mezayen, A.M., Shahin, H.A., and Kawady, N.A., *J. Radioanal. Nucl. Chem.*, 2021, vol. 328, no. 2, pp. 539–550.
23. El-Fekya, M.G., Mohammed, H.S., El-Shabasy, A.M., Ahmed, M.R., Abdel-Monem, Y.K., and Mira, H.I., *Int. J. Environ. Anal. Chem.*, 2021.
<https://doi.org/10.1080/03067319.2021.1925262>
24. Anjos, R.M., Veiga, R., Soares, T., Santos, A.M.A., Aguiar, J.G., Frascá, M.H.B.O., Brage, J.A.P., Uzêda, D., Mangia, L., Facure, A., Mosquera, B., Carvalho, C., and Gomes, P.R.S., *Radiat. Meas.*, 2005, vol. 39, no. 3, pp. 245–253.
25. Heikal, M.T.S., Abd, M., Monsef, E., Goma, S.R., Mansi, E., and Top, G., *J. Environ. Hazards*, 2018, vol. 2, no. 1, article 111.
26. El-Taher, A., Kamel, M., Tolba, A., and Salaheldin, G., *Radiat. Detect. Technol. Meth.*, 2020, vol. 5, no. 1, pp. 15–26.
27. El-Galy, M.M., *Geology, Radioactivity, Geochemistry and Tectonic Setting of Selected Granitic Rocks, West Gulf of Aqaba, Sinai, Egypt*, Tanta (Egypt): Tanta Univ., 1998.
28. Shalaby, M.H., *Bull. Fac. Sci. Alex. Univ.*, 1995, vol. 35, no. 2, pp. 447–460.
29. El Galy, M.M. and El Mowafy, A.A., *Egypt. J. Geol.*, 2003, vol. 47, no. 2, pp. 787–811.
30. El-Qassas, R.A.Y. and Abu-Donia, A.M., *Arab. J. Geosci.*, 2019, vol. 12, article 707.
<https://doi.org/10.1007/s12517-019-4902-2>
31. Saunders, D.F. and Potts, M.J., *Manual for Application of NURE 1974–1977 Aerial gamma-Ray Spectrometric Data, Report GJBX-13 (87)*, US Department of Energy, Grand Junction Office, 1978.
32. Efimov, A.V., *Multiplicative Parameter for Revealing Endogenic Ores from Aerogamma-Spectrometric Data, Methods of Ore Geophysics*, Preprint of the Geofizika Research and Production Association, Leningrad, 1978.
33. Gnojek, I. and Přichystal, A., *Geoexploration*, 1985, vol. 23, no. 4, pp. 491–502.